American Journal of Biomedicine and Pharmacy
https://biojournals.us/index.php/AJBP
ISSN: 2997-7177

Antibacterial Efficacy of the Phyto-Fabricated Chitosan and Chitosan-Based Silver Nanoparticles against *Acinetobacter Baumannii* Isolates Antibacterial Resistance

Sajjad Mohsin Irayyif
College of Dentistry, Department of Basic Sciences, Wasit University, Iraq
salazawi@uowasit.edu.iq

Received: 2024, 15, Feb
Accepted: 2025, 21, Mar
Published: 2025, 30, Apr

Annotation: Background and Aim: Healthcare-associated infections are caused by Acinetobacter baumannii. Despite being an opportunistic disease, A. baumannii infections are famously challenging to treat because of acquired and innate antibiotic resistance, which frequently restricts the range of feasible treatment choices. In the medical setting, A. baumannii can persist for extended periods of time, especially on inanimate surfaces. In order to compare the use of chitosan (ChNPs), silver nitrate (AgNPs), and phytofabricated chitosan-based silver nitrate (GNPs) nanoparticles in the medical field, this study was conducted.

Methods: The methanolic flower extract of Spathodea campulata was used to create the nanoparticles in an environmentally friendly manner. FTIR, SEM, NTA, and UV-visible spectroscopy were used to characterize the produced nanoparticles.

Antibacterial activities of the NPs were demonstrated against isolates of Acinetobacter baumannii in vitro by using well diffusion, MIC, MBC, ROS generation test, COMET assay, and qPCR.

Results: According to our data, the different absorption ranges for the nanoparticles were as follows: AgNPs, CHNPs, and GNPs

displayed absorption peaks at 345 nm, 320 nm, and 482 nm, respectively. The average size of the synthesized NPs, as determined by the SEM examination, was 76 nm for ChNPs, 90 nm for AgNPs, and 65 nm for GNPs. According to the broth dilution assay, the MIC for GNPs and the positive control was 48.3µg/ml and 25.6µg/ml, respectively. The MBC values for GNPs and the positive control were 23.4 µg/ml and 6.8 µg/ml, respectively. Following treatment with AgNPs at both concentrations, ROS production significantly increased in comparison to the control and positive control ($P<0.05$). A clear pattern of DNA damage was evident in the generated NPs at ½ MIC concentration ($P<0.05$). Based on the relative expression data, we discovered that all three members of the outer membrane protein gene (OmpA, Omp33, and OmpW) had dramatically decreased expression after treatment ($P<0.05$). This study shows that the produced nanoparticle has the potential to be a strong antimicrobial agent.

Keywords: Acinetobacter baumanii, ROS production, Spathodea campulata, Chitosan, qPCR, COMET assay.

Introduction:

Healthcare-associated infections are caused by *Acinetobacter baumannii*. Despite being an opportunistic disease, *A. baumannii* infections are famously challenging to treat because of acquired and innate antibiotic resistance, which frequently restricts the range of feasible treatment choices. In the medical setting, *A. baumannii* can persist for extended periods of time, especially on inanimate surfaces. Such settings should be taken into consideration as a significant component of infection control procedures since they may serve as a reservoir for cross-colonization and infection outbreaks. Furthermore, nosocomial bacteria may spread through healthcare workers' attire and devices (Chapartegui-González I, 2018).

Only a small number of putative virulence factors have been linked to the pathophysiology of *A. baumannii* illness, despite the fact that more than 80 whole genome sequences of various strains have been released. A capsular polysaccharide and the outer membrane protein (OmpA) appear to play a role in virulence or the contact with epithelial cells in vitro [Vila-Farres X, 2015]. Both in vitro and in vivo, other surface elements or secreted proteins have a negligible impact. It has been proposed that the fulminant course of the disease may be caused by an excessive host response to *A. baumannii* lipopolysaccharide, given these few virulence factors [Wong D, 2017].

Because *A. baumannii* can become resistant to all classes of antibiotics, like other non-fermentative Gram-negative bacilli, and because the number of multi-drug resistant (MDR) isolates is rapidly rising, physicians are being forced to employ colistin and other antibiotics as a last choice [Garnacho-Montero J,, 2015]. Numerous investigations revealed the existence of this

pathogen in a range of medical settings, where direct contact with infected patients or indirect contact with contaminated inanimate surfaces are the two main ways that *A. baumannii* is spread [Shamsizadeh Z, 2017]. Crucially, ICU-acquired infections may be significantly influenced by the cross-transmission of microbes from abiotic surfaces [Russotto V, 2015]. The ability of *A. baumannii* to tolerate desiccation and hunger appears to be a significant element in its spread in these conditions [Espinal P, 2012]. Additionally, it has the ability to create biofilms, which are bacterial communities encased in a protective polymeric matrix [Bravo Z, 2018]. Another possible virulence factor is the bacterium's capacity to form biofilms, which raises its survival rate on dry surfaces and may help it remain in hospital settings, raising the risk of nosocomial infections and outbreaks [Bravo Z, 2018].

Even though the relationship between contamination, *Acinetobacter* survival in the patient care setting, and the risk of infections linked to healthcare has not yet been proven, understanding the mechanisms underlying this pathogen's long-term persistence in hospital settings is essential to halting clonal spread and creating new targets for diagnostic and treatment tests.

N-acetyl-D-glucosamine and D-glucosamine units joined by β-1,4-glycosidic bonds form the natural cationic biopolymer known as chitosan (CS) [Chandrasekaran M, 2020]. The antibacterial activity of CS has been investigated in earlier research, and more recently, many CS derivatives have been created to strengthen the compound's inherent antibacterial properties. Other remarkable biological properties of CS include nontoxicity, biocompatibility, and biodegradability. These have made it beneficial in a variety of industries, including food, medicine, textiles, cosmetics, and agriculture [Kong, M.; 2010].

As nanotechnology increases the capacity to extend antibacterial research to the atomic level, it has begun to play an increasingly significant role among the amazing advancements in biological technologies and chemical identification techniques [Ma, Z., 2017]. A derivative of CS with superior physicochemical qualities are chitosan nanoparticles (CS-NPs). Numerous techniques, including ionotropic gelation, microemulsion, emulsification solvent diffusion, polyelectrolyte complex, and the reverse micellar method, have been used to create CS-NPs [Divya, K, 2017]. Communication with either the bacterial cell wall or the cell membrane is most likely the mechanism of CS-NPs' antibacterial activity. Various theories have been put forth to explain this mechanism. The electrostatic interaction between the positively charged amino groups of glucosamine and the negatively charged bacterial cell membranes is the most well-known CS-NPs paradigm of antimicrobial activity [Nguyen, V.B, 2016]. Through this interaction, the cell surface undergoes widespread changes that alter membrane permeability, which in turn triggers osmotic imbalance and intracellular chemical efflux, ultimately leading to cell death [Birsoy, K, 2015].

Additionally, chitosan nanoparticles were added to antimicrobial textiles for medical applications5. Additionally, chitosan nanoparticles were employed in insecticide7, fungicide treatment9, herbicide delivery for weed eradication [Maruyama, C. R., 2016], and nanofertilizer for plants' balanced nutrition. The medical pathogens Escherichia coli, Klebsiella pneumoniae, Pseudomonas aeruginosa, and Staphylococcus aureus10 are all effectively combatted by chitosan nanoparticles (Divya, K., 2017).

Common pathogens called Acinetobacter baumannii strains can result in serious nosocomial infections that are contracted in hospitals, especially in intensive care units. These infections can include skin infections, soft-tissue infections in burn patients, bacteremia, pneumonia, and urinary tract infections [Kröger, C., 2017]. Furthermore, one of the main bacterial infections, Acinetobacter baumannii strains, can form a biofilm. Tetracyclines, carbapenems, aminoglycosides, fluoroquinolones, and other extended-spectrum β-lactam antibiotics are among the groups of antibiotics to which biofilms are resistant [Pourhajibagher, M, 2020].

Therefore, developing new methods to prevent and cure infections brought on by strains of *Acinetobacter baumannii* that form biofilms is essential.

The green production of chitosan based nanoparticles from chitosan solution utilizing extract from *Spathodea campulata* flowers was the primary focus of this investigation. Additionally, the biosynthesized nanoparticles were characterized, and the antibacterial activity of the CNPs was assessed against *Acinetobacter baumannii* that forms biofilms. Antibacterial activity was evaluated by antibacterial resistance assays and gene expression studies.

Methods:

Green synthesis of Nanoparticles: For the green synthesis of the Silver nanoparticles, methanol extract of *Spathodea campulata* was used. In brief, about 5gm of the flowers of *Spathodea campulata* were homogenized in a mortar using pestle and added to 200ml of methanol and incubated in a water bath at 40^0C for 8hr. Following incubation, the contents were incubated in dark for overnight and filtered. The filtrate was then concentrated in a rotary evaporator and weighed for the yield. About 50mg of this powdered form was then re-dissolved in 50ml of de-ionized water and added to 50ml of 3mM of silver nitrate. The contents were then kept for stirring on a magnetic stirrer for one hour. The pH was adjusted to 9 with 0.1N NaOH. Nanoparticles were prepared as per the protocol described by Maheo, A. R *et al* (2022) but with minor modifications.

In parallel, about 20ml of chitosan solution was added to the methanol and silver nitrate solution and kept for stirring at 55°C until the colour change. Colour change confirms the formation of green synthesized nanoparticles (GNPs). Chitosan solution was prepared by adding 20mg of chitosan in glacial acetic acid (1.5%) solution. After centrifuging the mixture for 20min at 10,000rpm, the nanoparticles were separated and washed thrice with de-ionized water and dried in a hot air oven at 70^0C. A similar procedure was used for the synthesis of Silver (AgNPs) and chitosan nanoparticles (ChNPs). Silver nitrate and chitosan were reduced with sodium tetraborohydrate ($NaBH_4$) for the formation of NPs.

Characterization of synthesized NPs: By using a UV spectrophotometer (Shimadzu, 1800) to record the nanoparticles' UV–visible spectra in the 200–800nm range, the production of the nanoparticles was verified. On a Perkin Elmer Spectrum One FTIR spectrophotometer (Bomem MB100) with a range of 3600–400cm^{-1}, Fourier transform infrared (FTIR) spectra was obtained using the KBr pellet method. Using FESEM-EDX (SEM; PhilipsXL30ESEM), the atomic ratio and surface morphology of the GNPs were ascertained. The DLS approach was used to screen the hydrodynamic size (Z average), zeta potential, and polydispersity index (PDI) of the produced AgNPs using a Horiba SZ-100 analyzer. X-ray diffraction analysis was used to confirm the nanoparticles' crystallinity (STOE-Germany). Cu Kα rays at 2θ ranged from 10° to 80° to measure the diffraction pattern.

Antibacterial activity:

Agar well diffusion: In short, a bacterial culture (5×10^4 CFU/ml) was injected into 20ml of LB agar medium that had been chilled to 55°C and then transferred onto petri plates. After setting, each well that had been punched in the agar was filled with roughly 20µL of samples. About 50µg/ml of the antibiotic Colistin sulfate was used as a positive control. After incubating for 24hr at 37°C, the plates were checked for inhibitory zones. In addition to the negative control (sterile distilled water), GNPs, AgNPs, and ChNPs were investigated. The inhibition zone diameter of the sample divided by the inhibition zone diameter of the positive control and multiplied by 100 is the percentage of inhibition (Rojas, J.J, 2006).

MIC and MBC: About 10µl of *A. baumanii* isolate was injected in LB broth to test the GNPs' bactericidal action. MIC calculations were used to identify GNPs' antibacterial activity. Briefly put, 10ml of Luria Bertani broth were inoculated with overnight isolate ($1x10^5$ CFU/ml) in test tubes. Each tube was then filled with GNPs solutions at different concentrations, ranging from 5µg/ml to 80µg/ml. The tubes were incubated at 37°C for the entire night while being shaken at 120rpm. Each tube's increase in optical density at 600nm (UV-Vis spectrophotometer, Shimadzu

1800) was used to evaluate the development of bacteria. As a positive control, 50µg/ml of colistin sulphate was utilized. AgNPs and ChNPs were assessed using comparable concentration ranges. The technique outlined by Mouzaki, M. et al. (2022) was used to determine the minimum inhibitory concentration (MIC). Any agent's minimum inhibitory concentration (MIC) is the lowest concentration at which planktonic cell proliferation is inhibited or stopped. The GNPs-treated bacterial culture was inoculated onto LB agar plates and incubated for 24hours at 37°C, and the minimum bactericidal concentration (MBC) was determined in order to confirm the antibacterial activity. The MBC is the lowest NP concentration at which bacteria on agar plates do not grow visibly (Pramanik A, 2012).

Drug resistance study: Using roughly 15 passages of ½ MIC measurements, the drug resistance of the microorganisms brought on by the antibacterial drugs was examined. About 10ml of fresh medium was incubated with 100µl of the bacterial suspension (10^5 CFU/mL, overnight) from the sub-MIC well at 37°C. This was the first passage in which the bacteria were exposed to treatments (GNPs, ChNPs, and P). After incubation, 10ml of new medium (without treatments) was injected with around 100µL of the bacterial suspension exposed to treatments from the ½ MIC well, and the mixture was incubated for 24hr at 37°C. After surviving the first round of treatments, the bacteria were subjected to another round of treatment and utilized in passage 2. In order to investigate drug resistance after a relatively long exposure to the antibacterial agent, 15 passes were conducted using surviving bacteria that had been exposed to AgNPs. Any increase in MIC that coincided with an increase in the number of passages after such numerous exposures to the antibacterial agent would be indicative of bacterial drug resistance (Ikai, H., 2013).

Reactive Oxygen Species (ROS) generation: With minor adjustments, method followed by Choi *et al.* (2015) method was used to assess the amount of reactive oxidative species (ROS) released by the bacterium. To put it briefly, a conical flask was filled with roughly 50ml of the culture and its corresponding treatments. The isolate was cultured at 37°C in a shaker with approximately 1ml of the treatments (GNPs, ChNPs, and positive control). Treatment was done at two varying concentrations of ½ and ¼ MIC. Following a 6-hour incubation period, the culture was centrifuged for 10min at 8000rpm, and the resulting pellet was mixed with 2% Nitro Blue Tetrazolium (NBT). The resulting pellet was centrifuged at 8000rpm for 10min after being incubated in the dark. After that, the pellet was centrifuged once more for five minutes at 8000rpm after being cleaned with PBS (pH 6.8). To break down the cell membrane, around 2ml of KOH (2M) solution were added to the suspension. After adding about 1ml of sterile distilled water to the suspension, it was allowed to sit at room temperature for 10min. Following another centrifugation, about 100µl of the supernatant was transferred to 96-well plates. An ELISA plate reader (Genetix) was used to measure the absorbance of the plate at 620 nm.

DNA fragmentation by comet assay: About Five ml of isolate at density of 10^4 cfu/ml were mixed with 1ml of treatments (GNPs, P, ChNPs) separately at ½ MIC concentration. For about 5hr, the isolates were incubated at 37°C while being constantly shaken at 200 rpm. Following 5min of spinning at maximum speed, the bacterial cells were pelleted, and the manufacturer's instructions for utilizing the Genomic DNA kit (HiMedia) to extract the bacterial DNA were followed. A gel documentation system (Biobase) was used to view the bands after the extracted DNA were loaded onto a 1.2% agarose gel in TAE buffer.

Real time PCR assay: To screen the expression patterns of the outer membrane proteins under the treatment of the synthesized NPs we sued qPCR assay.

Treatment and RNA extraction: To 100ml of LB media, 20µl of the bacterial isolate was introduced, followed by 10µl of the corresponding treatments at a ½ MIC concentration. The positive control tube was filled with 10µl of Colistin (1/2 MIC). The control is the untreated tube. After that, the contents were incubated for 24 to 48 hours at 37°C. Following incubation, the cultures were centrifuged, and the resulting pellet was utilized to extract RNA. We carried out the process as directed by the RNeasy Kit.

cDNA synthesis: cDNA was synthesized using the RT PCR kit (SuperScript TMII Reverse Transcriptase; 200U/µl (HiMedia). The concentration of RNA achieved was roughly 2.08µg/µl, as such the reaction utilized approximately 1.21µl of RNA, random primers and 1µl of RT enzyme. The mixture was then incubated at 25°C for 10min after being mixed thoroughly. After 45 min of incubation at 65°C, the resulting cDNA was kept until it was needed for gene expression analysis.

Table 1: List of primers for the outer membrane proteins used for the qPCR study.

Primer		**Sequence (5'->3')**	Length	Tm	GC%	Product
ompA (ID: 92893473)	FW	CCGCTCCAAATGGATGGAGT	20	60.23	55	140
	RV	TCCCGGTCAGTTCAAATCGG	20	58.7	55	
omp33 (ID: 92893473)	FW	GCTAGCCATGACCGGTGCTC	20	60.18	55	340
	RV	AGCTTCGCCATCGTTACCAA	20	60.04	50	
	RV	TGGGTTATAACGGCGGTGAC	20	60.11	55	
ompW (ID: 92892291)	FW	GTAAAATTTGGGGGCAGCGT	20	59.39	50	320
	RV	TGATCCGCCTTTACCACACC	20	60.04	55	
16S rRNA	FW	TCAGCTCGTGTCGTGAGATG	20	54.5	50	240
	RV	CGTAAGGGCCATGATG	16	52.4	52	

Real-time PCR: Using primer3 software, real-time primers (Table 1) were created and purchased from Sigma-Aldrich. According to Sudhakar Malla *et al.* (2020), the real-time PCR experiment was performed using the iQTM SYBR Green Supermix (HiMedia). Primers (600nM) and 1µl of the RT products were used in the PCR test, yielding a 25µl total reaction volume. The Corbett Research cycler (Bio-Rad) was used to quantify the samples (control and treatment) on a thermocycler. About 40 cycles of the program were run, including 55 seconds at 92°C, 55 seconds at 62°C, and a 55-second elongation step at 72°C. The housekeeping gene 16srRNA and the relevant gene of interest were amplified in order to conduct the comparative analysis of the mRNA expression. The $\Delta\Delta^{Ct}$ technique was used to quantify the fold expression of the mRNA levels.

Statistical analysis:

All of the data in this study was displayed as mean ± SD. To assess the comparative differences between samples, a two-way ANOVA was performed. A p-value of less than 0.05 was deemed statistically significant.

Results:

Characterization of synthesized NPs:

From our data, the various absorption ranges for the nanoparticles were found to be 345nm, 320nm, and 482 nm for AgNPs, CHNPs, and GNPs showed absorption peaks at respectively. The change in the solution's hue is the main sign that the biogenesis of noble metal nanoparticles was effective. As a result, the solution's hue rapidly changed from a light yellow to a dark brown as a result of the bioreduction. The characteristic absorbance peak in the UV-vis spectrum that is larger than 400nm is used in the literature as a confirmation index for the synthesis of AgNPs (Varadavenkatesan, T., 2020).

From the SEM analysis we found the average size of the synthesized NPs to be 76nm, 90nm and 65nm respectively for ChNPs, AgNPs and GNPs. Form the SEM we could find the particle shape to be spherical in shape.

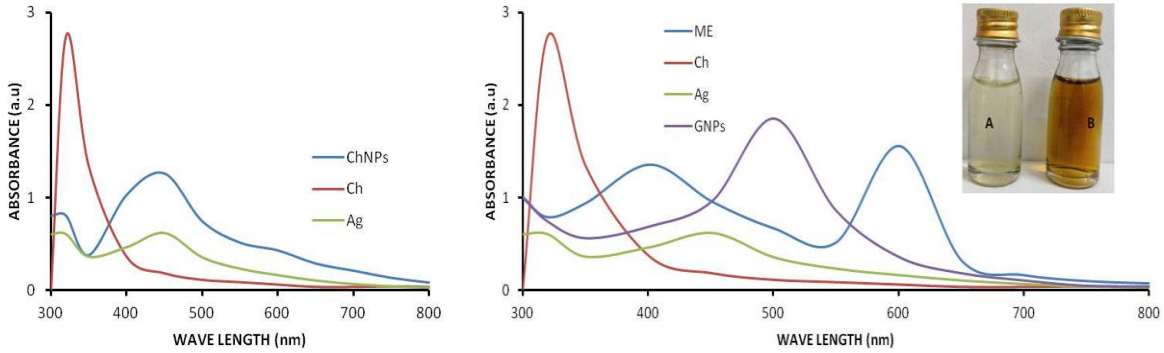

Figure 1: UV spectra of the syntheszied NPs. ChNPs: Chitosan NPs, ME: Methanol extract; GNPs: Green synthesized NPs.

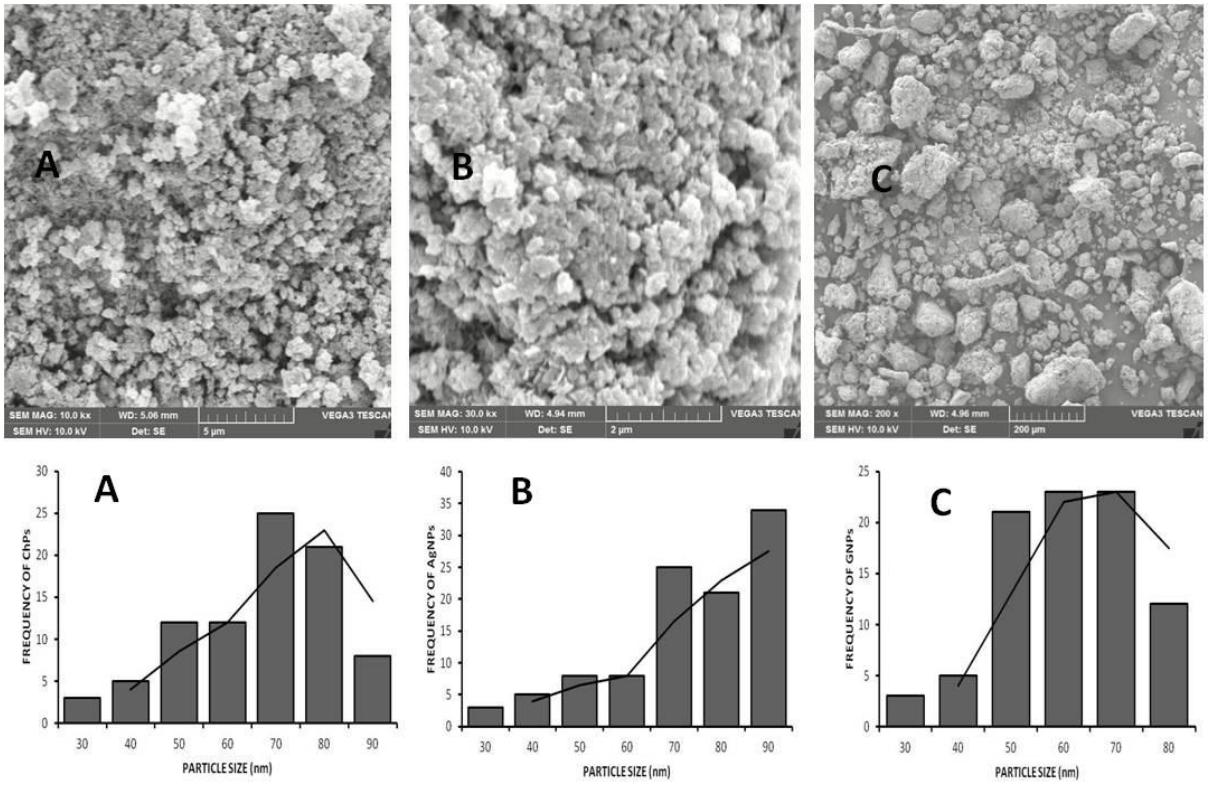

Figure 2: Images taken from SEM for the A: ChNPs, B: AgNPs; C: GNPs. Below graphs demonstrating the particle size of the NPs can be seen.

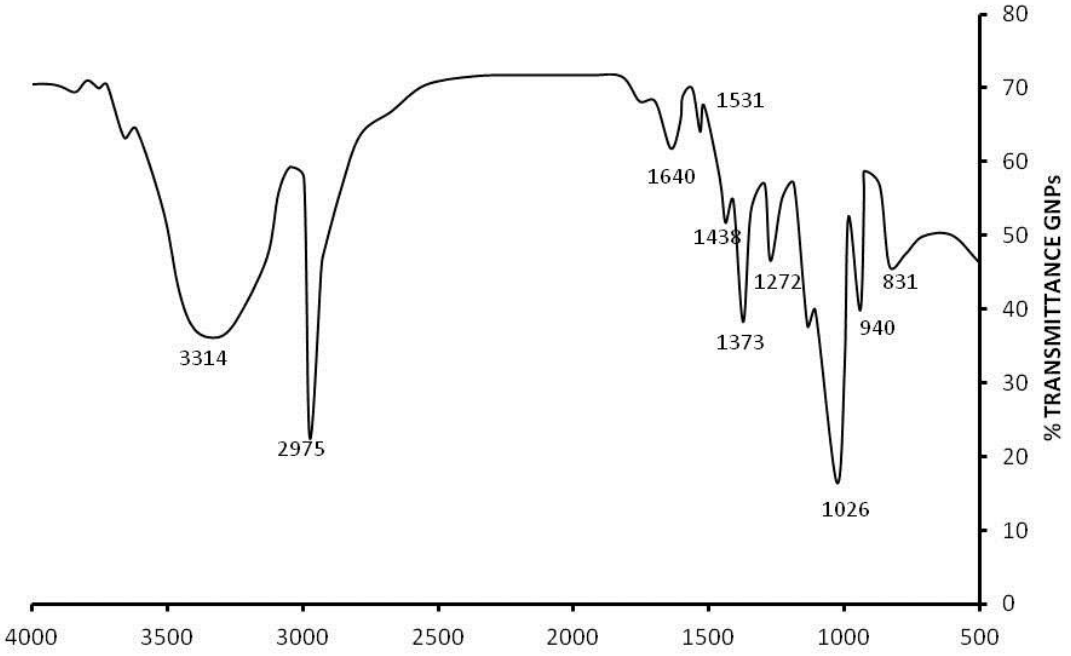

Figure 3: FTIR spectra of the GNPs.

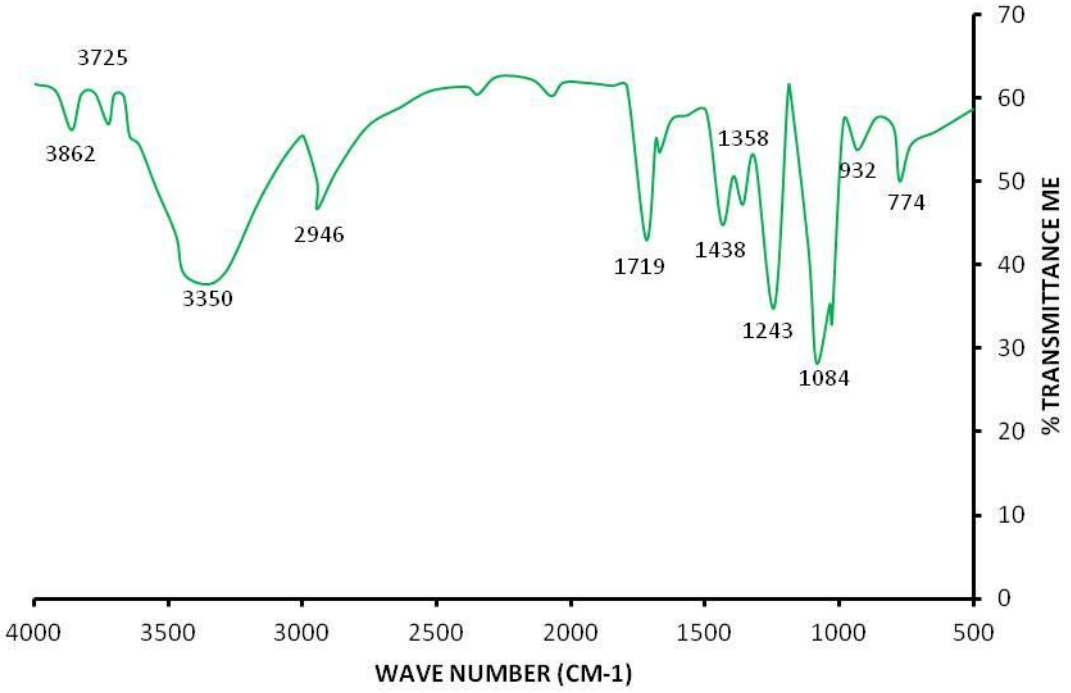

Figure 4: FTIR spectra of the Methanol extract.

Because of the intramolecular hydrogen bonds, the relatively broad vibrational bands seen in the 3350–2946cm^{-1} range correspond to N–H and O–H stretching. Around 2975cm^{-1}, the aliphatic C–H symmetric stretching absorption bands are visible. The presence of the carbonyl group (C=O) may be verified at 1640cm^{-1}. The presence of the primary amine in chitosan and the remaining amide of peptide in floral extract are confirmed by a medium signal of N–H bending vibrations centered at 1531cm^{-1}. The C-N stretching of the amino acid molecule is responsible for the appearance of a rather significant absorption peak at 1373cm^{-1}. The sharp bands at 1026 and 940cm^{-1} correlate to stretching of C–O. The C-O-C bending vibrations in glycosidic bonds are the source of the infrared band at 831cm^{-1}.

Antibacterial activity: From the data we could find a significant antibacterial activity by both well diffusion and broth dilution method. From the well diffusion method, we found the inhibition zones to be 13.45 ± 1.14, 5.6 ± 0.16, 3.5 ± 0.21 for the GNPs, ChNPs and AgNPs respectively. On the other hand, positive control showed 16.5 ± 0.87 mm inhibition zone ($P<0.05$). The percent inhibition as calculated with respect to positive control was found to be 82, 34 and 21% respectively for GNPs, ChNPs and AgNPs ($P<0.05$).

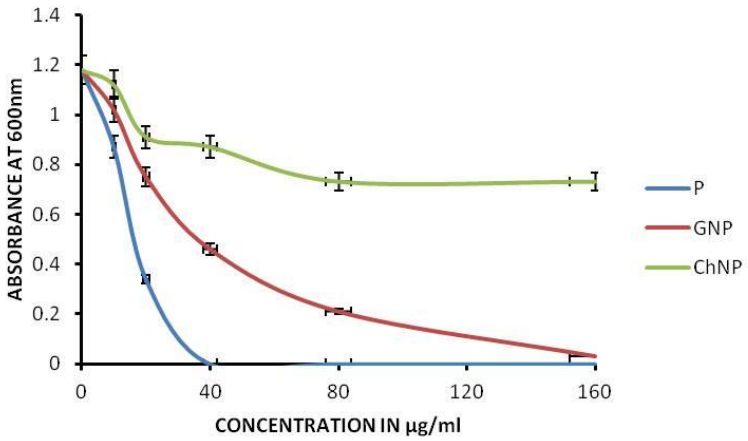

Figure 5: Line graph showing the OD600 of the isolates under the treatment of varying concentrations of positive control (P), GNPs and ChNPs.

We found GNPs can effectively inhibit the growth of *A. baumanii* as confirmed from MIC and MBC. We found that GNPs can inhibit bacteria at a MIC concentration of 48.3µg/ml, whereas ChNPs and AgNPs showed a MIC of > 125 against the bacterial isolate ($P<0.05$). In contrast, positive control can totally inhibit bacteria at a lower MIC (25.6µg/ml). We also calculated the MBC of each NP; the MBC for GNPs was 23.4µg/ml, which is highly significant when compared to the positive control ($P<0.05$), and the MBC for the positive control was the lowest (6.8µg/ml). The consistent MBC and MIC data suggest that the synthesized NPs have antibacterial properties.

Bacterial drug resistance assay: Following exposure to GNPs and respective positive control the serial MICs of planktonic strains were determined for 15 passages. The ½ MIC was found in the previous section to be 12.5, 25 and 59µg/ml respectively for positive control, GNPs and ChNPs against *A.baumanii*. The ½ MIC value of positive control (12.5µg/ml) changed to 14.5µg/ml at 12^{th} passage to 13^{th} passage and changed to 14.8 and 15.6µg/ml at 14^{th} and 15^{th} passage respectively ($P<0.05$). On the other hand, GNPs maintained the resistance till 13^{th} generation (Figure 6). The MIC value of NPs (25µg/ml) changed to 26.8 and 28µg/ml at 14^{th} and 15^{th} passage respectively ($P<0.05$). With this we could confirm that the isolate showed susceptibility to NPs till 14^{th} generations, while the positive control showed till 13^{th} generation (Figure 6). This confirms the antibacterial nature of the green synthesized AgNPs. While, ChNPs showed resistance after 10^{th} passage with a change in MIC from 59µg/ml to 65µg/ml and 68µg/ml at 11^{th} and 13^{th} passage respectively ($P<0.05$) (Figure 7).

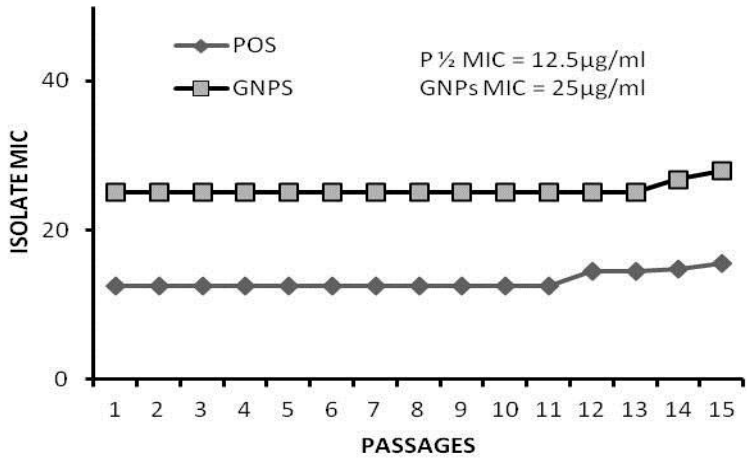

Figure 6: Bacterial drug resistance assay of GNPs. ½ MIC was measured from passages 0 to 15. POS: Positive control. ½ MIC values can be seen in the graph.

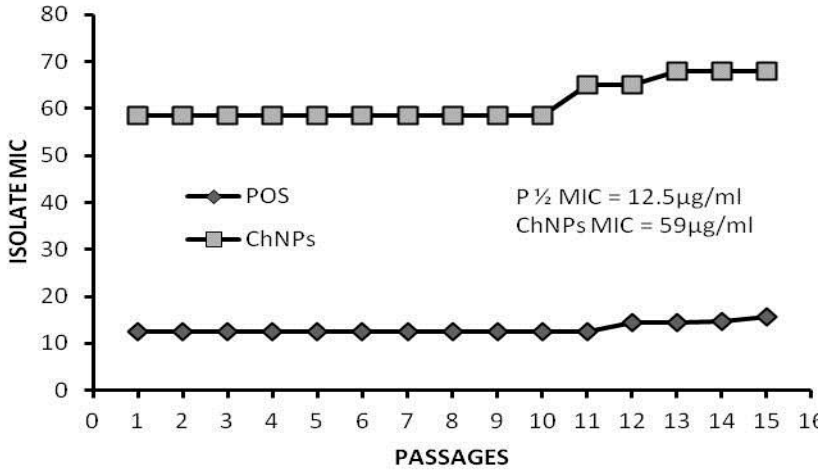

Figure 7: Bacterial drug resistance assay of ChNPs. ½ MIC was measured from passages 0 to 15. POS: Positive control. ½ MIC values can be seen in the graph.

Reactive Oxygen Species (ROS) generation: Reactive oxygen species (ROS) production causes excessive oxidative stress, which damages proteins, lipids, membranes, and DNA/RNA. Cytotoxic effects in prokaryotic cells are exacerbated as a result. In order to compare the ROS levels in this isolate to the negative control (DMSO), ROS generation was assessed by treating it with GNP, ChNP, and positive control. When compared to the control and positive control, there was a notable increase in ROS generation following treatment with AgNPs at both concentrations ($P<0.05$) (Figure 8). The production of ROS was found to be 55 and 76% at ¼ MIC and ½ MIC respectively when treated with GNPs ($P<0.05$). On the other hand, the positive control showed 72 and 78% of ROS production at ¼ MIC and ½ MIC respectively. ChNPs showed 38 and 67% respectively at ¼ and ½ MIC concentrations ($P<0.05$). ROS production with GNPs was highly significant when compared to positive control.

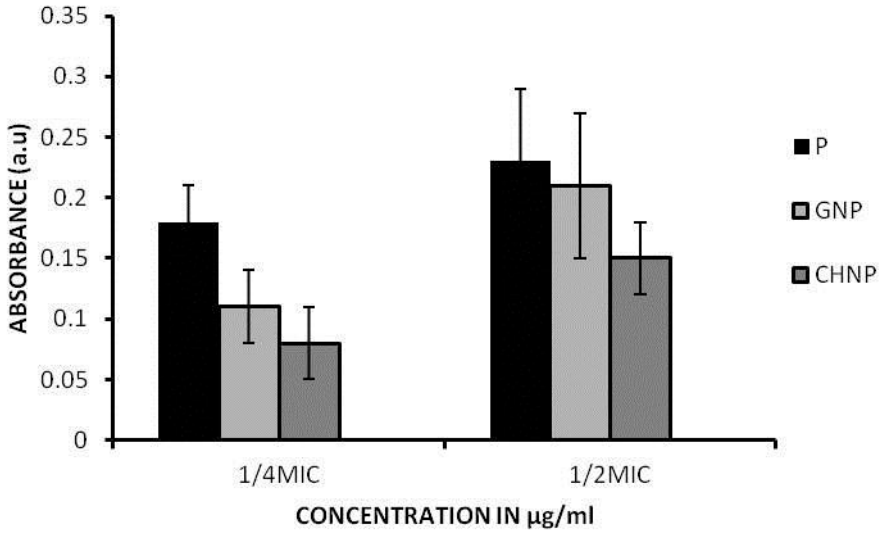

Figure 8: ROS assay: Production of ROS under the treatment of NPs. P: Positive control.

DNA fragmentation: Representative pictures of DNA fragmentation analysis on gel electrophoresis were shown in Figure 5. The produced NPs at ½ MIC concentration showed a distinct pattern of DNA damage ($P<0.05$). The control band was seen to be distinct and clear. The amount of DNA found in the positive control was insufficient, and the damage was evident from the DNA shearing (Figure 9). The concentration was directly correlated with the damage. When compared to the control and positive control, the GNPs' similar banding pattern validates the GNPS's considerable activity ($P<0.05$).

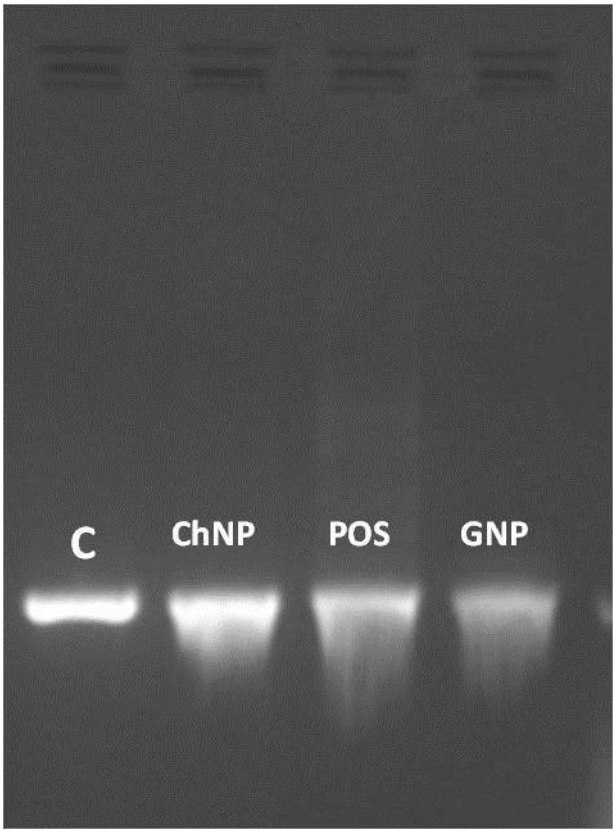

Figure 9: COMET assay showing the DNA damage. C: Control; POS: Positive control.

qPCR analysis: From the relative expression data obtained, we found all the 3 outer membrane protein gene members were significantly downregulated post treatment ($P<0.05$). A down regulation was with ompA gene member, where the expression was found to be 22% and 44%

respectively for NPs and positive control ($p<0.05$). Similarly Omp33 gene member, was found to be down regulated where the expression was found to be 13% and 44% respectively for NPs and positive control ($p<0.05$). A down regulation was with ompW gene member, where the expression was found to be 50% and 58% respectively for NPs and positive control ($p<0.05$). The results were found to be highly significant when compared to controls (control was assumed 1 or 100%) (Figure 12-16).

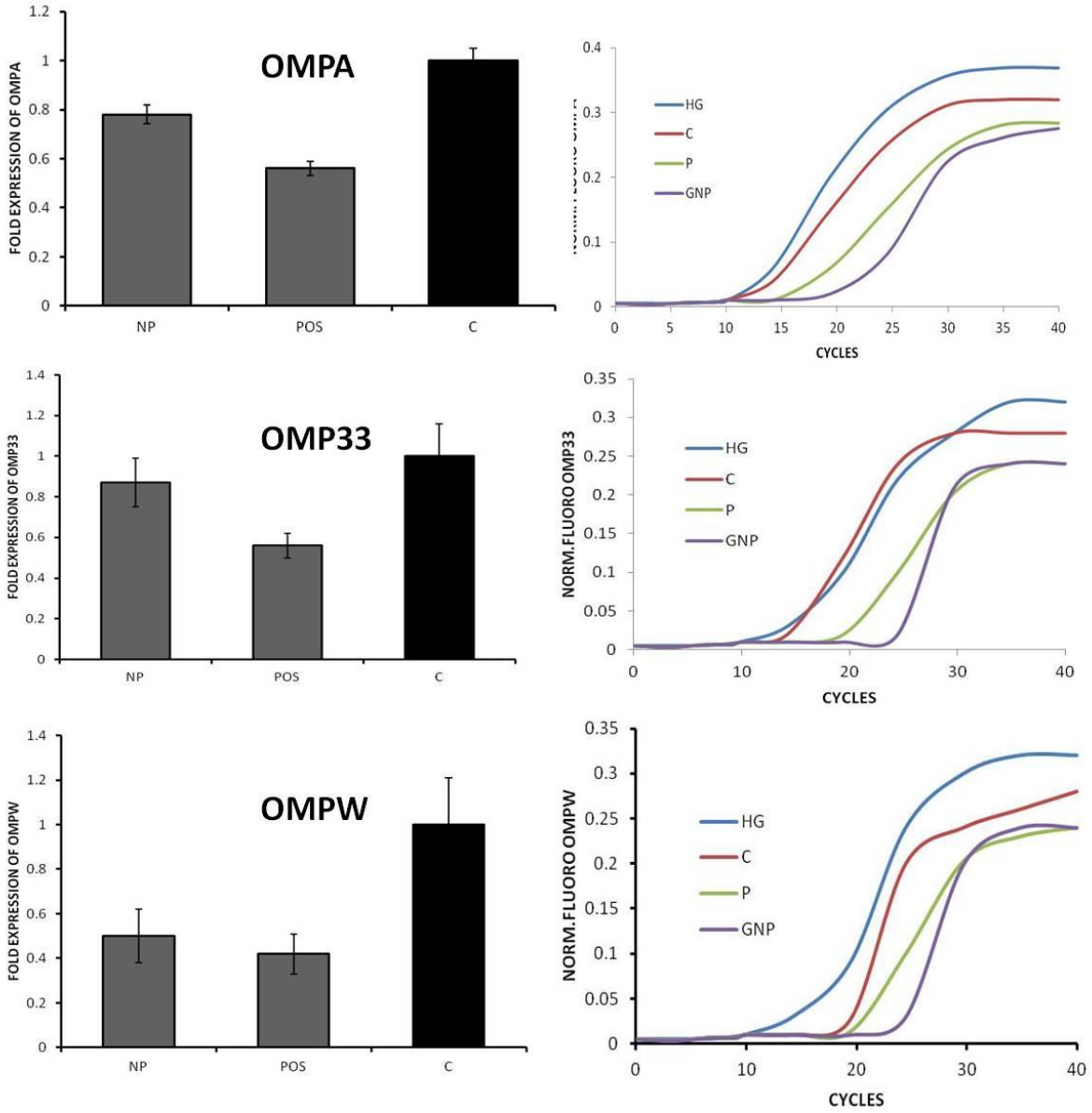

Figure 10: Real time PCR analysis. Fold expression histograms (left) for the gene members and the Ct curves for the gene members (Right) are represented. P: positive control; C: Control (Without treatment).

Discussion:

Enhancing chitosan performance with nanoparticles is an active research topic. We assessed the combined effects of phyto fabricated CSNPs *A. baumanii* antibacterial resistance because of CSNPs' capacity to disrupt the biofilm structure. CSNPs were made from low-molecular-weight chitosan for this investigation.

According to our data, the different absorption ranges for the nanoparticles were as follows: AgNPs, CHNPs, and GNPs displayed absorption peaks at 345 nm, 320 nm, and 482 nm, respectively. The characteristic absorbance peak in the UV-vis spectrum that is larger than

400nm is used in the literature as a confirmation index for the synthesis of AgNPs (Varadavenkatesan, T., 2020).

The average size of the synthesized NPs, as determined by the SEM examination, was 76nm for ChNPs, 90nm for AgNPs, and 65nm for GNPs. We could determine from the SEM that the particles had a spherical form.

The morphology of all nanoparticles was relatively homogeneous, with a quite consistent particle size distribution and spherical in shape. The SEM analysis indicates spherical particles with a smooth surface. Similar results were reported by El-Naggar, et al (2022).

We found similar banding pattern of the CSNPs to the previous reports. The sharp bands at 1026 and 940cm^{-1} correlate to stretching of C–O. The C-O-C bending vibrations in glycosidic bonds are the source of the infrared band at 831cm^{-1}. The presence of flavones, terpenoids, and polysaccharide components in the extract causes the in-plane O-H bending of aromatic compounds, which is associated with peaks at 1026–940cm^{-1} (Olajire, A. A. 2020). Similar –NH_2 bending vibration78 was represented by the peak at 1568cm^{-1} by Rajam, M., et al (2011). Because of the intramolecular hydrogen bonds, the relatively broad vibrational bands seen in the 3350–2946cm^{-1} range correspond to N–H and O–H stretching. Similar pattern (Peaks between 3400 and 3800cm^{-1}) was observed in the report (Damiri, F., 2020).

By using both the broth dilution method and well diffusion, we were able to determine a considerable antibacterial activity from the data. For GNPs, ChNPs, and AgNPs, the corresponding percent inhibition, as determined in relation to the positive control, was 82, 34, and 21% ($P<0.05$). By preventing the formation of biofilms and possibly boosting the effectiveness of antibiotics, chitosan-based nanoparticles exhibit promise as antibacterial agents against *Acinetobacter baumannii*, especially multi-drug resistance strains (Abdeltwab, W. M., 2019). One of *Acinetobacter baumannii's* well-known traits is its capacity to create antibiotic-resistant biofilms. Chitosan nanoparticles have demonstrated efficacy in inhibiting the formation of biofilms, particularly when mixed with other substances such as copper oxide (CuO) or iron oxide (Fe3O4) [Sarfraz Muhammad Hassan, 2023]. By attaching itself to the negatively charged bacterial cell wall, chitosan nanoparticles can possibly damage the cell membrane and change its permeability, potentially causing cell death by obstructing DNA replication [Sarfraz Muhammad Hassan, 2023].

We found GNPs can effectively inhibit the growth of *A. baumanii* as confirmed from MIC and MBC. We found that GNPs can inhibit bacteria at a MIC concentration of 48.3µg/ml, whereas ChNPs and AgNPs showed a MIC of > 125 against the bacterial isolate ($P<0.05$). AgNPs based on chitosan efficiently stop the growth of A. baumannii, even the strains that are resistant to multiple drugs [Sarfraz Muhammad Hassan, 2023]. According to studies, AgNPs can increase antibiotics' effectiveness against A. baumannii, possibly lowering the requirement for large doses of the drug [Silva Santos K., 2016]. Because of their possible synergistic effects with antibiotics, chitosan-based silver nanoparticles (AgNPs) exhibit promise as antibacterial agents against *Acinetobacter baumannii*, including strains that are resistant to several drugs, by preventing the formation of biofilms and bacterial growth (El-Naggar, *et al*, 2022). But we report for the first time, the efficacy of these CSNPs fabricated with *Spathodea* flower extract.

From the drug resistance assays, we found the isolate exhibited NP susceptibility up to the fourteenth generation, whereas the positive control did so up to the thirteenth generation (Figure 6). This demonstrates that the green produced AgNPs are antimicrobial. With a change in MIC from 59µg/ml to 65µg/ml and 68µg/ml at the 11th and 13th passages, respectively ($P<0.05$), GNPs demonstrated resistance after the 10th passage (Figure 7). Antibiotic resistance assays were reported by the biologists, but a very few papers stand in support of the efficacy of the AgNPs with chitosan against *A.baumanii*. moreover, these CSNPs were further phyto fabricated with extract from *Spathodea campulata.*

When treated with GNPs, ROS generation was observed to be 55 and 76% at ¼ MIC and ½ MIC, respectively ($P<0.05$). In comparison to the positive control, ROS generation with GNPs was highly significant. Excessive oxidative stress brought on by the generation of reactive oxygen species (ROS) harms proteins, lipids, membranes, and DNA/RNA. This exacerbates cytotoxic effects in prokaryotic cells. MDR isolates and pathogens that produce biofilms are among the many Gram-positive and Gram-negative organisms against which ROS have shown a strong antibacterial effect both in vitro and in vivo [Dryden, M., 2017]. When applied topically to skin, mucosal membranes, or interior tissue that may be infested with microbial populations and biofilms, ROS may offer a novel treatment strategy [Dryden, M.S, 2017]. In addition to being clinically licensed for the treatment of infected wounds, treatments utilizing ROS as antimicrobial agents are already available for topical application and are undergoing development for clinical usage in additional contexts [Dunnill, C, 2017].

From the comet assay also, we found the produced NPs at ½ MIC concentration showed a distinct pattern of DNA damage ($P<0.05$). The control band was seen to be distinct and clear. The amount of DNA found in the positive control was insufficient, and the damage was evident from the DNA shearing (Figure 9). DNA fragmentation assay was marked as the effective invitro assay to detect the efficacy of the Nanoparticles when treated against bacterial and cancer lines [Gurunathan S, 2013, Zhang G, 2011].

From the relative expression data obtained, we found all the 3 outer membrane protein gene members were significantly downregulated post treatment ($P<0.05$). A down regulation was seen with gene member, where the expression was found to be 22%, 13% and 50% respectively for ompA Omp33 ompW gene members. Therapeutic approaches may target *Acinetobacter baumannii* since downregulation of OmpA (outer membrane protein A) has been associated with decreased virulence, decreased biofilm formation, and maybe decreased antibiotic resistance. OmpA is the most well researched virulence factor among those *A. baumannii* OMPs, and it is crucial in controlling the host's immunological response as well as the adhesion, aggression, and biofilm formation of *A. baumannii*. An independent risk factor for the mortality rate of nosocomial pneumonia and bacteremia brought on by *A. baumannii* is an excess of OmpA [Sanchez-Encinales V, 2017]. Additionally, OmpA expression levels determined by qRT-PCR can serve as a quick diagnostic indicator for antibiotic-resistant *A. baumannii*, and the outcomes are quite similar to those obtained using conventional MIC analysis [Martin-Pena R, 2013]. Research indicates that omp gene member disruption may result in lower minimum inhibitory concentrations (MICs) of some antibiotics [Smani Y, 2014].

In *Acinetobacter baumannii*, downregulation of the omp33 gene results in decreased lethality in a mouse model as well as decreased fitness and virulence, including compromised adherence, invasion, and cytotoxicity [Rumbo C, 2014]. The outer membrane protein (OMP) Omp33 (or Omp33-36) in *A. baumannii* serves as a porin, a channel that allows water and other tiny molecules to pass through. It contributes significantly to the bacterium's capacity to produce infections and is linked to carbapenem resistance [Smani Y, 2014]. OmpW is essential for bacterial pathogenicity and may be a target for novel treatments. In Acinetobacter baumannii, downregulation of the outer membrane protein OmpW, a virulence factor, results in decreased biofilm formation and lower bacterial loads in a mouse sepsis model (Schmitt, B.L., 2023). Research has demonstrated that A. baumannii strains that have OmpW downregulated (i.e., its expression is decreased) generate biofilms far less frequently than strains of the wild type [Gil-Marqués ML, 2022].

Conclusion: In order to ascertain the nanoparticles' potential as antibacterial agents against *Acinetobacter baumannii*, this study examined their effectiveness when created using a green method. The antibacterial and antibiofilm properties of the chitosan-based nanoparticles (GNPs) were assessed. The GNPs demonstrated efficacious actions against strains of *Acinetobacter baumannii* and inhibited the outer membrane proteins, both of which can significantly impact hospital infection management. The powerful properties of the produced nanoparticles were

additionally validated by the COMET assay, ROS generation, and antibacterial resistance bioassays. The results of our investigation indicate that GNPs may find use in the medical field, and we draw the conclusion that these nanoparticles may be the most promising option for treating infections that are resistant to several drugs. To fully understand the potential activities and cytotoxicity of the nanoparticles in real-world situations, as well as the difficulties associated with their large-scale commercial production, more in vivo studies are advised.

References:

1. Abdeltwab, W. M., Abdelaliem, Y. F., Metry, W. A., and Eldeghedy, M. (2019). Antimicrobial effect of chitosan and nano-chitosan against some pathogens and spoilage microorganisms. *J. Adv. Lab. Res. Biol.* 10, 8–15.
2. Birsoy, K.; Wang, T.C.; Chen, W.W.; Freinkman, E.; Abu-Remaileh, M.; Sabatini, D.M. An essential role of the mitochondrial electron transport chain in cell proliferation is to enable aspartate synthesis. *Cell* 2015, *162*, 540–551.
3. Bravo Z, Chapartegui-Gonzalez I, Lazaro-Diez M, Ramos-Vivas J. *Acinetobacter pittii* biofilm formation on inanimate surfaces after long-term desiccation. J Hosp Infect. 2018;98(1):74–82. pmid:28764931.
4. Chandrasekaran M, Kim KD, Chun SC. Antibacterial Activity of Chitosan Nanoparticles: A Review. *Processes*. 2020; 8(9):1173. https://doi.org/10.3390/pr8091173
5. Chapartegui-González I, Lázaro-Díez M, Bravo Z, Navas J, Icardo JM, Ramos-Vivas J (2018) *Acinetobacter baumannii* maintains its virulence after long-time starvation. PLoS ONE 13(8): e0201961. https://doi.org/10.1371/journal.pone.0201961
6. Choi, H., Yang, Z., and Weisshaar, J. C. (2015). Single-cell, real-time detection of oxidative stress induced in *Escherichia coli* by the antimicrobial peptide CM15. *Proc. Natl. Acad. Sci. U.S.A.* 112, E303–E310. doi: 10.1073/pnas.1417703112
7. Damiri, F., Bachra, Y., Bounacir, C., Laaraibi, A. & Berrada, M. Synthesis and characterization of lyophilized chitosan-based hydrogels cross-linked with benzaldehyde for controlled drug release. *J. Chem.* 2020(8747639), 1–10 (2020).
8. Divya, K., Vijayan, S., George, T. K. & Jisha, M. S. Antimicrobial properties of chitosan nanoparticles: Mode of action and factors affecting activity. *Fibers Polymers* 18(2), 221–230 (2017).
9. Dryden, M. Reactive Oxygen Therapy: A Novel Therapy in Soft Tissue Infection. *Curr. Opin. Infect. Dis.* 2017, *30*, 143–149. [Google Scholar] [CrossRef] [PubMed]
10. Dryden, M.S.; Cooke, J.; Salib, R.J.; Holding, R.E.; Biggs, T.; Salamat, A.A.; Allan, R.N.; Newby, R.S.; Halstead, F.; Oppenheim, B.; et al. Reactive Oxygen: A Novel Antimicrobial Mechanism for Targeting Biofilm-Associated Infection. *J. Glob. Antimicrob. Resist.* 2017, *8*, 186–191. [Google Scholar] [CrossRef]
11. Dunnill, C.; Patton, T.; Brennan, J.; Barrett, J.; Dryden, M.; Cooke, J.; Leaper, D.; Georgopoulos, N.T. Reactive Oxygen Species (ROS) and Wound Healing: The Functional Role of ROS and Emerging ROS-modulating Technologies for Augmentation of the Healing Process. *Int. Wound J.* 2017, *14*, 89–96. [Google Scholar] [CrossRef]
12. El-Naggar, N.EA., Shiha, A.M., Mahrous, H. *et al.* Green synthesis of chitosan nanoparticles, optimization, characterization and antibacterial efficacy against multi drug resistant biofilm-forming *Acinetobacter baumannii*. *Sci Rep* 12, 19869 (2022). https://doi.org/10.1038/s41598-022-24303-5
13. Espinal P, Marti S, Vila J. Effect of biofilm formation on the survival of *Acinetobacter baumannii* on dry surfaces. J Hosp Infect. 2012;80(1):56–60. pmid:21975219.

14. Garnacho-Montero J, Amaya-Villar R, Ferrandiz-Millon C, Diaz-Martin A, Lopez-Sanchez JM, Gutierrez-Pizarraya A. Optimum treatment strategies for carbapenem-resistant *Acinetobacter baumannii* bacteremia. Expert Rev Anti Infect Ther. 2015;13(6):769–77. pmid:25865094.

15. Gil-Marqués ML, Pachón J, Smani Y. iTRAQ-Based Quantitative Proteomic Analysis of Acinetobacter baumannii under Hypoxia and Normoxia Reveals the Role of OmpW as a Virulence Factor. Microbiol Spectr. 2022 Apr 27;10(2):e0232821. doi: 10.1128/spectrum.02328-21. Epub 2022 Mar 2. PMID: 35234505; PMCID: PMC8941935.

16. Gurunathan S, Han JW, Eppakayala V, Jeyaraj M, Kim JH. Cytotoxicity of biologically synthesized silver nanoparticles in MDA-MB-231 human breast cancer cells. Biomed Res Int. 2013;2013:535796. doi: 10.1155/2013/535796. Epub 2013 Jul 8. PMID: 23936814; PMCID: PMC3722883.

17. Ikai, H. *et al*. *In vitro* evaluation of the risk of inducing bacterial resistance to disinfection treatment with photolysis of hydrogen peroxide. *PLoS One* 8, e81316 (2013).

18. Kong, M.; Chen, X.; Xing, K.; Park, H.J. Antimicrobial properties of chitosan and mode of action: A state of the art review. *Int. J. Food Microbiol.* 2010, *144*, 51–63.

19. Kröger, C., Kary, S. C., Schauer, K. & Cameron, A. D. Genetic regulation of virulence and antibiotic resistance in *Acinetobacter baumannii*. *Genes* 8(1), 12 (2017).

20. Ma, Z.; Garrido-Maestu, A.; Jeong, K.C. Application, mode of action, and in vivo activity of chitosan and its micro- and nanoparticles as antimicrobial agents: A review. *Carbohydr. Polym.* 2017, *176*, 257–265.

21. Maheo, A. R., Vithiya, B. S. M., Prasad, T. A. A., Tamizhdurai, P., and Mangesh, V. (2022). Biosynthesis, characterization, biological and photo catalytic investigations of Elsholtzia blanda and chitosan mediated copper oxide nanoparticles. *Arab. J. Chem.* 15:103661. doi: 10.1016/j.arabjc.2021.103661

22. Martin-Pena R, Dominguez-Herrera J, Pachon J, McConnell MJ. Rapid detection of antibiotic resistance in Acinetobacter baumannii using quantitative real-time PCR. J Antimicrob Chemother. 2013;68:1572–5.

23. Maruyama, C. R. *et al.* Nanoparticles based on chitosan as carriers for the combined herbicides imazapic and imazapyr. *Sci. Rep.* 6(1), 1–15 (2016).

24. Mouzaki, M., Maroui, I., Mir, Y., Lemkhente, Z., Attaoui, H., El Ouardy, K., Lbouhmadi, R. & Mouine, H. (2022). Green synthesis of silver nanoparticles and their antibacterial activities. *Green Processing and Synthesis*, *11*(1), 1136-1147. https://doi.org/10.1515/gps-2022-0061

25. Nguyen, V.B.; Nguyen, T.T.H.; Wang, S.-L.; Vo, T.P.K.; Nguyen, A.D. Preparation of chitosan nanoparticles by TPP ionic gelation combined with spray drying, and the antibacterial activity of chitosan nanoparticles and a chitosan nanoparticle–amoxicillin complex. *Res. Chem. Intermed.* 2016, *43*, 3527–3537.

26. Olajire, A. A. & Mohammed, A. A. Green synthesis of bimetallic Pd core Au shell nanoparticles for enhanced solid-phase photodegradation of low-density polyethylene film. *J. Mol. Struct.* 1206, 127724 (2020).

27. Pourhajibagher, M., Hosseini, N., Boluki, E., Chiniforush, N. & Bahador, A. Photoelimination potential of chitosan nanoparticles-indocyanine green complex against the biological activities of *Acinetobacter baumannii* strains: A preliminary in vitro study in burn wound infections. *J. Lasers Med. Sci.* 11(2), 187 (2020).

28. Pramanik A, Laha D, Bhattacharya D, Pramanik P, Karmakar P. A Novel Study of Antibacterial Activity of Copper Iodide Nanoparticle Mediated by DNA and Membrane Damage. Colloids Surf B Biointerfaces. 2012; 96: 50–55. pmid:22521682

29. Rajam, M., Pulavendran, S., Rose, C. & Mandal, A. B. Chitosan nanoparticles as a dual growth factor delivery system for tissue engineering applications. *Int. J. Pharm.* 410(1–2), 145–215 (2011).

30. Rumbo C, Tomás M, Fernández Moreira E, Soares NC, Carvajal M, Santillana E, Beceiro A, Romero A, Bou G. The Acinetobacter baumannii Omp33-36 porin is a virulence factor that induces apoptosis and modulates autophagy in human cells. Infect Immun. 2014 Nov;82(11):4666-80. doi: 10.1128/IAI.02034-14. Epub 2014 Aug 25. PMID: 25156738; PMCID: PMC4249306.

31. Russotto V, Cortegiani A, Raineri SM, Giarratano A. Bacterial contamination of inanimate surfaces and equipment in the intensive care unit. J Intensive Care. 2015;3:54. pmid:26693023.

32. Sanchez-Encinales V, Alvarez-Marin R, Pachon-Ibanez ME, Fernandez-Cuenca F, Pascual A, Garnacho-Montero J, Martinez-Martinez L, Vila J, Tomas MM, Cisneros JM, Bou G, Rodriguez-Bano J, Pachon J, Smani Y. Overproduction of outer membrane protein a by Acinetobacter baumannii as a risk factor for nosocomial pneumonia, bacteremia, and mortality rate increase. J Infect Dis. 2017;215:966–74.

33. Sanchez-Encinales V, Alvarez-Marin R, Pachon-Ibanez ME, Fernandez-Cuenca F, Pascual A, Garnacho-Montero J, Martinez-Martinez L, Vila J, Tomas MM, Cisneros JM, Bou G, Rodriguez-Bano J, Pachon J, Smani Y. Overproduction of outer membrane protein a by Acinetobacter baumannii as a risk factor for nosocomial pneumonia, bacteremia, and mortality rate increase. J Infect Dis. 2017;215:966–74.

34. Sarfraz Muhammad Hassan , Zubair Muhammad , Aslam Bilal , Ashraf Asma , Siddique Muhammad Hussnain , Hayat Sumreen , Cruz Jorrdy Neves , Muzammil Saima , Khurshid Mohsin , Sarfraz Muhammad Farrukh , Hashem Abeer , Dawoud Turki M. , Avila-Quezada Graciela Dolores , Abd_Allah Elsayed Fathi. Comparative analysis of phyto-fabricated chitosan, copper oxide, and chitosan-based CuO nanoparticles: antibacterial potential against Acinetobacter baumannii isolates and anticancer activity against HepG2 cell lines. Frontiers in Microbiology. VOL 14, 2023 DOI=10.3389/fmicb.2023.1188743.

35. Schmitt, B.L., Leal, B.F., Leyser, M. *et al.* Increased *ompW* and *ompA* expression and higher virulence of *Acinetobacter baumannii* persister cells. *BMC Microbiol* 23, 157 (2023). https://doi.org/10.1186/s12866-023-02904-y

36. Shamsizadeh Z, Nikaeen M, Nasr Esfahani B, Mirhoseini SH, Hatamzadeh M, Hassanzadeh A. Detection of antibiotic resistant *Acinetobacter baumannii* in various hospital environments: potential sources for transmission of *Acinetobacter* infections. Environ Health Prev Med. 2017;22(1):44. pmid:29165152.

37. Silva Santos K., Mendonça Barbosa A., da Costa L.P., Santos Pinheiro M., Prior Pinto Oliveira M.B., Pad F.F. Silver nanocomposite biosynthesis: Antibacterial activity against multidrug-resistant strains of Pseudomonas aeruginosa and Acinetobacter baumannii. Molecules. 2016;21:1255. doi: 10.3390/molecules21091255.

38. Smani Y, Dominguez-Herrera J, Pachón J. Association of the outer membrane protein Omp33 with fitness and virulence of Acinetobacter baumannii. J Infect Dis. 2013 Nov 15; 208(10):1561-70. doi: 10.1093/infdis/jit386. Epub 2013 Aug 1. PMID: 23908480.

39. Smani Y, Fàbrega A, Roca I, Sánchez-Encinales V, Vila J, Pachón J. Role of OmpA in the multidrug resistance phenotype of Acinetobacter baumannii. Antimicrob Agents Chemother.

2014;58(3):1806-8. doi: 10.1128/AAC.02101-13. Epub 2013 Dec 30. PMID: 24379205; PMCID: PMC3957889.

40. Varadavenkatesan, T., Selvaraj, R. & Vinayagam, R. Green synthesis of silver nanoparticles using *Thunbergia grandiflora* flower extract and its catalytic action in reduction of Congo red dye. *Mater. Today Proc.* 23, 39–42 (2020).Return to ref 29 in article

41. Vila-Farres X, Ferrer-Navarro M, Callarisa AE, Marti S, Espinal P, Gupta S, et al. Loss of LPS is involved in the virulence and resistance to colistin of colistin-resistant *Acinetobacter nosocomialis* mutants selected *in vitro*. J Antimicrob Chemother. 2015;70(11):2981–6. pmid:26311838.

42. Wong D, Nielsen TB, Bonomo RA, Pantapalangkoor P, Luna B, Spellberg B. Clinical and Pathophysiological Overview of *Acinetobacter* Infections: a Century of Challenges. Clinical microbiology reviews. 2017;30(1):409–47. pmid:27974412.

43. Zhang G, Lai BB, Zhou YY, Chen BA, Wang XM, Lu Q, Chen YH. Fe3O4 nanoparticles with daunorubicin induce apoptosis through caspase 8-PARP pathway and inhibit K562 leukemia cell-induced tumor growth in vivo. Nanomedicine. 2011 Oct;7 (5):595-603. doi: 10.1016/j.nano.2011.01.013. Epub 2011 Feb 17. PMID: 21333751; PMCID: PMC3132242.